Maximum Efficiency Operation of Wireless In-Wheel Motor Using Pulse Amplitude Modulation

Daiki Tajima*a) Student Member, Kensuke Hanajiri*b) Student Member
Osamu Shimizu*c) Non-member, Hiroshi Fujimoto*d) Senior Member

The authors' research group invented a Wireless In-Wheel Motor (W-IWM) in order to overcome the low reliability of In-wheel motor's power and signal wires. We have developed its control methods to stabilize the load voltage. Using those control methods, load voltage can be adjustable. In this paper, maximum efficiency operation by adjusting load voltage to an optimal value is proposed. Optimal load voltage is derived from motor and inverter efficiency models and the characteristic of wireless power transfer system. Experiments verify that the proposed method improves efficiency of W-IWM system.

Keywords: Wireless power transfer, Magnetic resonance coupling, In-Wheel motor, Pulse amplitude modulation

1. Introduction

In recent years, electric vehicles (EVs) have attracted attention for their less harmful emissions. EVs have a very quick torque response provided by motors compared to the internal combustion engine vehicles [1]. Moreover, In-wheel motor (IWM) type EVs drive each wheel independently. They can provide safer and more comfortable driving [2] [3]. Furthermore, optimizing each wheel's torque distribution, consumption energy can be minimized [4] [5].

However, conventional IWMs have a risk of disconnection of the power and signal cables connecting the IWM to the vehicle body. Those cables are exposed to harsh environment and may be damaged due to continuous bending, freezing in cold environment or impact caused by a debris colliding from the road.

To overcome the risk of disconnection, the authors' research group invented a Wireless In-Wheel Motor (W-IWM) in which the IWM receives its power wirelessly [6]. The test vehicle equipped W-IWM is shown in Fig. 1. Because of the misalignment between the motor and the vehicle side coil caused by steering and suspension vibration, wireless power transfer system using magnetic resonance coupling is employed. This method is robust to the misalignment between the transmitter and receiver coils. However, it is known that load voltage or current change with constant power load [7]. In order to realize W-IWM, stabilization control of the load voltage is proposed [8].

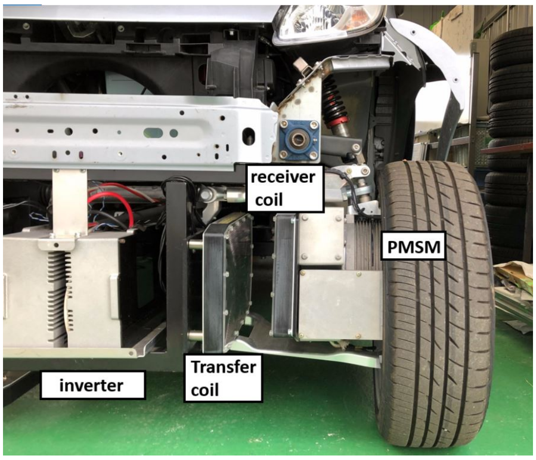

Fig. 1. W-IWM attached to the test vehicle.

In the previous study, load voltage is stabilized at a constant value [8]. Using same control method, it can be adjustable. In a previous study [9], the efficiency of whole powertrain is improved by optimizing the load voltage that maximizes motor and inverter efficiency using an additional buck-boost converter. The circuit configuration is shown in Fig. 2. This control method is called Quasi-PAM control. However, the loss due to the additional buck-boost converter is increased. In W-IWM system, it can be applied without extra buck-boost converter.

In the circuit configuration shown in Fig. 2, the optimal load voltage can be determined only considering the motor and inverter efficiency. However, considering W-IWM system, the load voltage should be larger than the voltage to transfer the required power.

In this paper, optimal load voltage is derived by motor, inverter, and WPT system models. And it is controlled by secondary side AC/DC converter. Experiments and simulation show that optimal load voltage adjustment improves efficiency of W-IWM system.

a) Correspondence to: tajima.daiki18@ae.k.u-tokyo.ac.jp
b) Correspondence to: hanajiri.kensuke17@ae.k.u-tokyo.ac.jp
c) Correspondence to: shimizu.osamu@edu.k.u-tokyo.ac.jp
d) Correspondence to: fujimoto@k.u-tokyo.ac.jp
* The University of Tokyo
5-1-5, Kashiwanoha, Kashiwa, Chiba, 277-8561 Japan
Phone: +81-4-7136-3881
Fax: +81-4-7136-3881

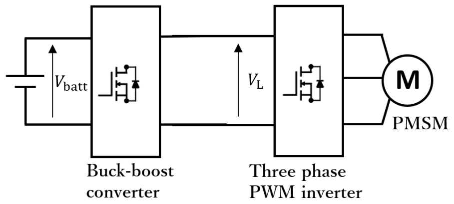

Fig. 2. Circuit configuration of powertrain with additional buck-boost converter.

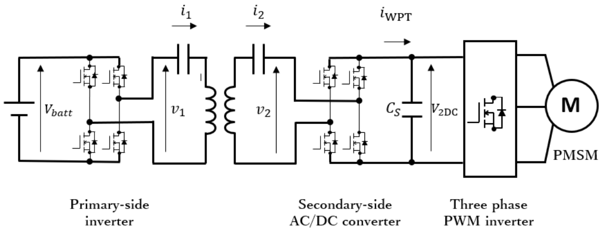

Fig. 3. Circuit configuration of W-IWM.

2. Circuit Structure and Modeling of W-IWM

2.1 Circuit Configuration In this research, the circuit configuration of W-IWM system shown in Fig. 3 is examined. Permanent Magnet Synchronous Motor (PMSM) is employed because of its high efficiency, high power factor, and high power density. The motor is driven by the voltage type three phase PWM inverter. Load voltage is the same as secondary side DC-link voltage V_{2DC} in this system. The method of WPT is Series-Series (S-S) magnetic resonance coupling because of its robustness against misalignment. Both primary side inverter and secondary side AC/DC converter are H-bridge circuits.

In this section, a model of PMSM is derived. Fig. 4 shows the d-axis and q-axis equivalent circuits of PMSM in the d-q coordinate [10]. From the circuits, the voltage equations of PMSM are expressed as

$$\begin{bmatrix} v_d \\ v_q \end{bmatrix} = R_a \begin{bmatrix} i_{od} \\ i_{oq} \end{bmatrix} + \left(1 + \frac{R_a}{R_c}\right) \begin{bmatrix} v_{od} \\ v_{oq} \end{bmatrix} \cdots\cdots\cdots\cdots (1)$$

$$\begin{bmatrix} v_{od} \\ v_{oq} \end{bmatrix} = \begin{bmatrix} 0 & -\omega_e L_q \\ \omega_e L_d & 0 \end{bmatrix} \begin{bmatrix} i_{od} \\ i_{oq} \end{bmatrix} + \begin{bmatrix} 0 \\ \omega_e \Psi \end{bmatrix} + \begin{bmatrix} 0 \\ \omega_e \Psi \end{bmatrix} + \frac{d}{dt} \begin{bmatrix} L_d & 0 \\ 0 & L_q \end{bmatrix} \begin{bmatrix} i_{od} \\ i_{oq} \end{bmatrix}. \cdots\cdots\cdots\cdots (2)$$

Mechanical output of PMSM P_{out} is given by

$$P_{out} = T_m \omega \cdots\cdots\cdots\cdots (3)$$

where T_m is motor torque. Neglecting d-axis current i_{od} for simplification, T_m is expressed as

$$T_m = P_n \Psi i_{oq} = K_t i_{oq} \cdots\cdots\cdots\cdots (4)$$

where Ψ is the interlinkage magnetic flux, and K_t is the torque coefficient.

2.2 Modeling of Inverter In this section, efficiency model of inverter is derived. Inverter loss consists of switching loss W_{sw} and conduction loss W_{on} of 6 switching devices. Therefore, total loss of the inverter is expressed as

$$W_{inv} = 6 \times (W_{sw} + W_{on}). \cdots\cdots\cdots\cdots (5)$$

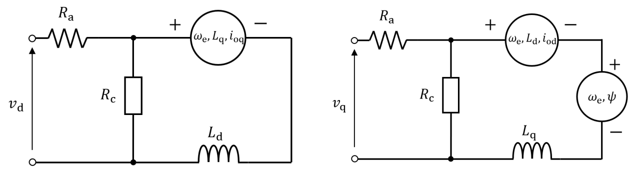

(a) d-axis. (b) q-axis.

Fig. 4. Equivalent circuits of Permanent Magnet Synchronous Motor.

Switching loss W_{sw} is written in the following form:

$$W_{sw} = \frac{1}{6} V_{2DC} I_{ave} (\Delta T_{on} + \Delta T_{off}) f_{sw} \cdots\cdots\cdots\cdots (6)$$

where V_{2DC} is the inverter input voltage, I_{ave} is the average current through the switching device, ΔT_{on} and ΔT_{off} are the time intervals during ON and OFF, f_{sw} is the switching frequency. Conduction loss is expressed as

$$W_{on} = V_{on} I_{ave} d \cdots\cdots\cdots\cdots (7)$$

where V_{on} is the Drain - Source voltage of the SiC switching device, d is duty ratio. From (6), it is found that the inverter loss increases as the secondary side DC link voltage V_{2DC} becomes larger.

3. Optimal Secondary Side DC-link Voltage

Total loss of the load W_L is expressed as following equation.

$$W_L = W_m + W_{inv} \cdots\cdots\cdots\cdots (8)$$

From (8), it can be seen that total loss of the load W_L decreases as the secondary side DC-link voltage V_{2DC} becomes lower. In this situation, optimal secondary side DC-link voltage is the lowest voltage at which the PMSM can be driven. The lowest voltage $V_{2DC_{min}}$ is given by

$$V_{2DC_{min}} = \sqrt{2}\sqrt{v_d^2 + v_q^2}. \cdots\cdots\cdots\cdots (9)$$

A method to control the voltage to the minimum value (optimal value) by feeding back the v_d and v_q can be considered. However, using feedback control, there is a possibility that the voltage transiently falls below the minimum value. Then, feedforward control is more desirable. Considering steady-state and equivalent iron loss resistance R_c is much larger than the armature winding resistance R_a, the voltage can be expressed as following equation

$$V_{2DC_{min}} = \sqrt{2}\sqrt{\left(\frac{R_a}{K_t} T_m + K_t \omega\right)^2 + \left(\frac{P_n \omega L_q}{K_t} T_m\right)^2}. \cdot (10)$$

It means the lower limit of the voltage (optimal voltage) can be estimated from the motor torque T_m and rotation speed ω. Using (10), required voltage can be calculated without v_d and v_q feedback. Then, secondary side DC-link voltage can be controlled to an optimal value by feedforward controller. However, electromotive force of L_d and L_q are ignored in the (10). Considering transient voltage, there is a possibility that the required voltage to operate PMSM is larger than the value calculated by (10). Therefore, secondary side DC-link voltage command $V_{2DC}{}^*$ need to be made by multiplying

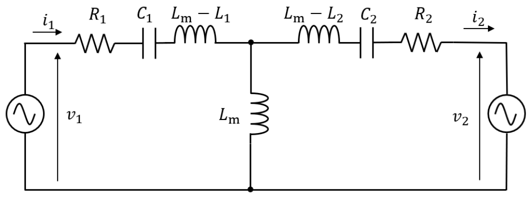

Fig. 5. Equivalent circuit of wireless power transfer via magnetic resonance coupling.

the (10) by a coefficient α to make a margin from the lower limit value. It can be expressed as

$$V_{2DC}{}^{*} = \alpha\sqrt{2}\sqrt{\left(\frac{R_a}{K_t}T_m + K_t\omega\right)^2 + \left(\frac{P_n\omega L_q}{K_t}T_m\right)^2}. \quad (11)$$

4. Secondary Side DC-link Voltage Control

4.1 Modeling of the Wireless Power Transfer System

The equivalent circuit of WPT system via magnetic resonance coupling is shown in Fig. 5. To fulfil the resonance condition, the operating frequency ω_0 is expressed as

$$\omega_0 = \frac{1}{\sqrt{L_1C_1}} = \frac{1}{\sqrt{L_2C_2}} \quad (12)$$

In the resonance condition, the impedance matrix of the equivalent circuit can be expressed as

$$Z = \begin{bmatrix} R_1 & j\omega_0 L_m \\ j\omega_0 L_m & R_2 \end{bmatrix} \quad (13)$$

The relationship between voltage and current on the primary side and the secondary side can be expressed by the following equation.

$$\begin{bmatrix} i_{11} \\ -i_{21} \end{bmatrix} = Z^{-1}\begin{bmatrix} v_{11} \\ v_{21} \end{bmatrix} \quad (14)$$

where i_{11}, i_{21}, v_{11}, and v_{21} are the fundamental harmonics of i_1, i_2, v_1, and v_2, respectively. In the WPT system, components other than the fundamental wave can be ignored because of its band pass characteristic. Then, we only focus on fundamental harmonics voltage and current. In this situation, transfer power can be expressed as

$$P_{WPT} = \frac{\omega_0 L_m V_{11}V_{21} + R_2V_{11}^2}{2(R_1R_2 + (\omega_0L_m)^2)} \quad (15)$$

where V_{11},V_{21},I_{11} and I_{21} are the amplitude of the fundamental harmonics of v_{11},v_{21},i_{11} and i_{21} respectively.

4.2 Control Method

In this section, a secondary side DC-link voltage control method is introduced. Primary side inverter outputs a rectangular wave which has $\pm V_{1DC}$ voltage amplitude shown in Fig. 6 (a). The amplitude of the fundamental harmonics voltage V_{11} is calculated as

$$V_{11} = \frac{4}{\pi}V_{1DC} \quad (16)$$

Fig. 6 (b) shows switching state of secondary side AC/DC converter. The duty ratio of the converter d_{conv} defined as $T_P/0.5T$ where T is periodic time, and T_P is time of the pulse width. Then, the amplitude of the fundamental harmonics

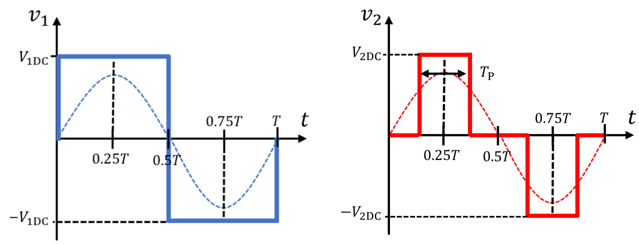

(a) Switching state of primary side inverter.

(b) Switching state of secondary side converter.

Fig. 6. Equivalent circuits of Permanent Magnet Synchronous Motor.

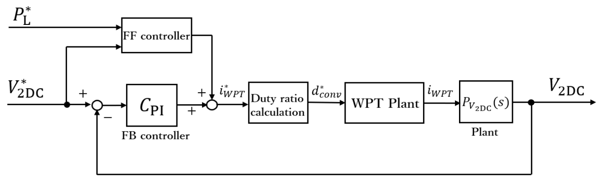

Fig. 7. Block diagram of secondary side DC-link voltage control.

voltage V_{21} is calculated as

$$V_{21} = \frac{4V_{2DC}}{\pi}\sin\frac{\pi d_{conv}}{2} \quad (17)$$

While the secondary side coil voltage v_2 is $\pm V_{2DC}$, secondary side coil current i_2 is rectified. Therefore, the secondary side AC-DC converter output current average $i_{WPT_{ave}}$ can be expressed as

$$\begin{aligned} i_{WPT_{ave}} &= \frac{1}{\pi}\int_{\frac{\pi}{2}+\frac{\pi}{2}d_{conv}}^{\frac{\pi}{2}-\frac{\pi}{2}d_{conv}} I_{21}\sin\theta d\theta \quad (18) \\ &= \frac{2}{\pi}I_{21}\sin\frac{\pi d_{conv}}{2} \end{aligned}$$

where I_{21} is the amplitude of the fundamental harmonics current i_{21}. Then, the relationship between duty ratio command $d_{conv}{}^{*}$ and converter output current command $I_{WPT}{}^{*}$ can be expressed as

$$d_{conv}{}^{*} = \frac{2}{\pi}\sin^{-1}\left(\frac{\pi I_{WPT}{}^{*}}{2I_{21}}\right) \quad (19)$$

The transfer function from the secondary side converter output current I_{WPT} to the secondary side DC-link voltage V_{2DC} is expressed as the following equation.

$$P_{V_{2DC}}(s) = \frac{V_{2DC}(s)}{I_{WPT}(s)} = \frac{R_L}{R_LC_ss + 1} \quad (20)$$

where, R_L is a equivalent resistance. And it can be expressed as

$$R_L = \frac{V_{2DC}^2}{P_L} \quad (21)$$

The relationship between load power command P_L^* and converter output current command $I_{WPT}{}^{*}$ can be expressed by the following equation.

$$I_{WPT}{}^{*} = \frac{P_L^*}{V_{2DC}^*} \quad (22)$$

The secondary side AC/DC converter controller is a two-degree-of freedom controller, the control target plant of which is $P_{V_{2DC}}$. We use a PI controller which is designed by the pole placement method.

$$\begin{aligned} C_{\mathrm{PI}}(s) &= K_{\mathrm{p}} + K_{\mathrm{i}}\frac{1}{s} \\ K_{\mathrm{p}} &= \frac{2pR_{\mathrm{L}}C_{\mathrm{s}}-1}{R_{\mathrm{L}}} \\ K_{\mathrm{i}} &= p^2C_{\mathrm{s}} \end{aligned} \quad \cdots\cdots (23)$$

where $-p$[rad/s] is a closed loop pole. When the secondary side DC-link voltage is controlled only by feedback controller, the responsiveness becomes worse. Therefore, feedforward controller is required. The output of the feedforward controller is calculated by (22). The block diagram of the secondary side DC-link voltage control is shown in Fig. 7.

4.3 Secondary Side DC-link Voltage Command The relationship between the secondary side DC-link voltage and the wireless transfer power can be expressed by the following equations derived from (15) and (17).

$$V_{21} = \frac{2(R_1R_2 + (\omega_0L_{\mathrm{m}})^2)P_{\mathrm{WPT}} - R_2V_{11}^2}{\omega_0L_{\mathrm{m}}V_{11}} \cdots\cdots (24)$$

$$V_{2\mathrm{DC}} = \frac{\pi}{4\sin\frac{\pi d_{\mathrm{conv}}}{2}}V_{21} \cdots\cdots (25)$$

Using the control method introduced in the previous chapter, it is necessary to make the secondary side DC-link voltage command larger than the voltage to transfer the required power. When d_{conv} is 1, transfer power is maximized. Therefore, the secondary side DC-link voltage command should be satisfied following equation.

$$V_{2\mathrm{DC}}^* > \frac{\pi}{4}\frac{2(R_1R_2 + (\omega_0L_{\mathrm{m}})^2)P_{\mathrm{WPT}} - R_2V_{11}^2}{\omega_0L_{\mathrm{m}}V_{11}} \cdots\cdots (26)$$

Wireless transfer power P_{WPT} can be estimated from torque T and rotation speed ω.

$$P_{\mathrm{WPT}} = \frac{1}{\eta_{\mathrm{L}}}P_{\mathrm{L}} = \frac{1}{\eta_{\mathrm{L}}}T\omega \cdots\cdots (27)$$

where P_{L} is motor output power and η_{L} is efficiency of PMSM. The voltage command derived from (11) should be satisfied following condition.

$$\begin{aligned} &\alpha\sqrt{2}\sqrt{\left(\frac{R_{\mathrm{a}}}{K_{\mathrm{t}}}T_{\mathrm{m}} + K_{\mathrm{t}}\omega\right)^2 + \left(\frac{P_{\mathrm{n}}\omega L_{\mathrm{q}}}{K_{\mathrm{t}}}T_{\mathrm{m}}\right)^2} \\ &> \frac{\pi}{4}\frac{2(R_1R_2 + (\omega_0L_{\mathrm{m}})^2)P_{\mathrm{WPT}} - R_2V_{11}^2}{\omega_0L_{\mathrm{m}}V_{11}} \cdots\cdots (28) \end{aligned}$$

If (28) is satisfied, the voltage command can be expressed as (11), else it can be expressed as following equation.

$$V_{2\mathrm{DC}}^* = \frac{\pi}{4}\frac{2(R_1R_2 + (\omega_0L_{\mathrm{m}})^2)P_{\mathrm{WPT}} - R_2V_{11}^2}{\omega_0L_{\mathrm{m}}V_{11}} \cdots\cdots (29)$$

5. Simulation

Simulation is conducted to verify the effectiveness to adjust secondary side DC-link voltage to an optimal value. Simulation conditions are determined considering the parameters

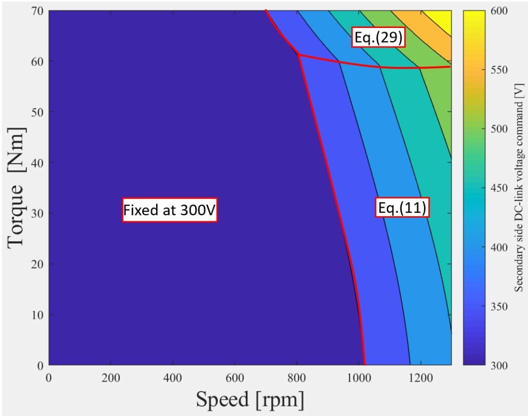

Fig. 8. Voltage command. (proposed method)

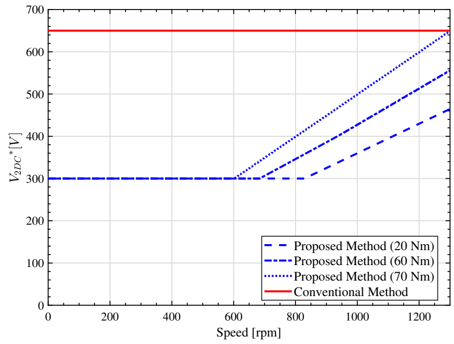

Fig. 9. Voltage command of the proposed method and conventional method.

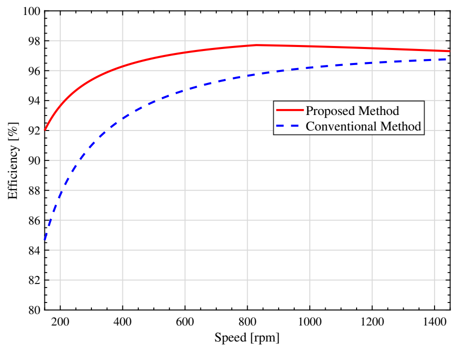

Fig. 10. Battery to inverter output efficiency in simulation. (torque is 20 Nm)

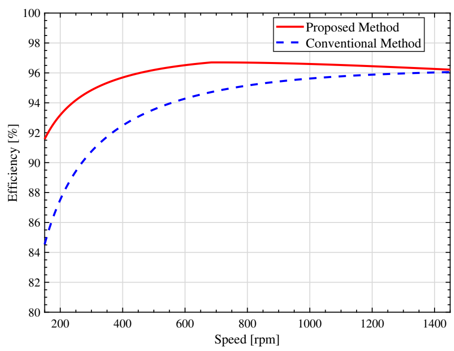

Fig. 11. Battery to inverter output efficiency in simulation. (torque is 60 Nm)

Table 1. Specifications of WPT system.

Resonance frequency	86.8 kHz
Switching frequency of DC/DC converter	86.8 kHz
Primary-side coil resistance R_1	242.0 mΩ
Primary-side coil inductance L_1	259.9μH
Secondary-side coil resistance R_2	242.0 mΩ
Secondary-side coil inductance L_2	259.9μH
Coil gap	100 mm
Coil mutual inductance L_m	58 μH
Smoothing capacitance C	1100 μF

of the experimental equipment shown in Table 1 and Table 2 and battery voltage $V_{1\mathrm{DC}}$ is 600 V.

In the conventional method, secondary side DC-link voltage command is fixed at 650 V to transfer sufficient power at the maximum output of the motor. On the other hand, it is variable in the proposed method. Substituting torque T_m and rotation speed ω into (11) and (28) yields the voltage command $V_{2\mathrm{DC}}^*$. In case of α is 1.2 and assuming η_PMSM is 0.85, the secondary side DC-link voltage command are shown in Fig. 8. Since the motor output fluctuates drastically in the low output range, the lower limit of the voltage command is fixed at 300 V. In the high power range, secondary side DC-link voltage command is restricted by (29). The efficiency from battery output to inverter output can be expressed as

$$\eta_\mathrm{all} = \eta_\mathrm{WPT}\frac{P_\mathrm{WPT} - W_\mathrm{inv}}{P_\mathrm{WPT}} \quad \cdots\cdots (30)$$

where η_WPT is the WPT efficiency. It can be expressed as

$$\eta_\mathrm{WPT} = \frac{\omega_0 L_\mathrm{m} V_{11} V_{21} - R_1 V_{21}^2}{\omega_0 L_\mathrm{m} V_{11} V_{21} + R_2 V_{11}^2} \quad \cdots\cdots (31)$$

The efficiency in the conventional method and the proposed method are calculated under the condition that the torque command value was fixed at 20 Nm and 60 Nm. In the proposed method, the secondary side DC-link voltage command is shown in Fig. 9. Substituting those voltage command into (30), the efficiency from primary side DC-link voltage to inverter output can be calculated. The calculation result is shown in Fig. 10 and Fig. 11. They show the effectiveness of the proposed method.

6. Experiment

Experiments are conducted to verify the effectiveness to adjust secondary side DC-link voltage to an optimal value.

6.1 Experimental Setup The equipment consists of a primary side DC power supply, a primary side inverter, transmitting and receiving coils, a secondary side converter, a voltage type three phase PWM inverter, and a Permanent Magnet Synchronous Motor. Instead of a battery, a regenerative DC power supply (pCUBE MWBFP 3-1250-J02: Myway) is used as the primary side voltage source. The primary side DC source voltage $V_{1\mathrm{DC}}$ is 600 V. The primary side inverter was a rectangular wave operation with a fixed duty ratio, and the operating frequency was 86.8 kHz. Secondary side converter synchronously rectifies with 86.8 kHz and controls secondary side DC-link voltage $V_{2\mathrm{DC}}$. Specifications of the WPT system used in W-IWM system is shown in Table 1. Specifications of the PMSM used in W-IWM system is shown in Table 3.

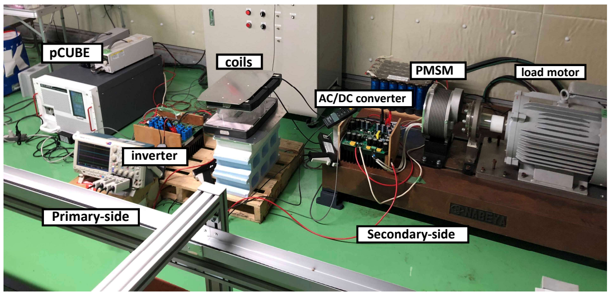

(a) Overall view.

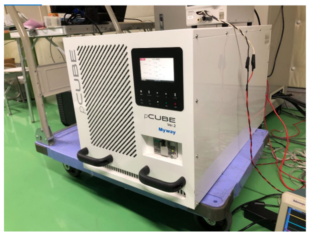

(b) pCUBE. (Voltage source)

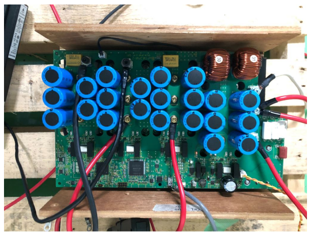

(c) Primary side inverter.

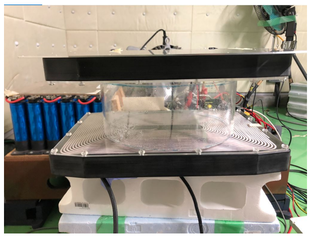

(d) Transmitter and receiver coils.

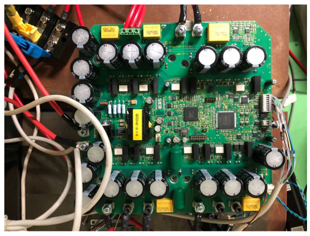

(e) Secondary side AC/DC converter.

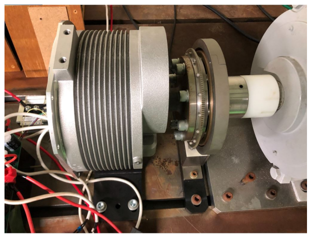

(f) PMSM.

Fig. 12. Experimental Setup.

Table 2. Specifications of three phase PWM inverter.

Turn on delay time	5.4 μs
Turn off delay time	3.0 μs
Drain-Source voltage of the SiC	6.0 mV

Table 3. Specifications of PMSM.

Rated power	15.6 kW
Rated speed	1500 rpm
Rated current	23.4 Arms
armature winding resistance per-phase R_a	606 mΩ
iron loss resistance R_c	50 Ω
flux linkage of permanent magnet Ψ	0.193Wb
Poles P_n	10
d-axis inductance L_d	0.359mH
q-axis inductance L_q	0.515mH

6.2 Comparison of Variable Voltage Method and Fixed Voltage Method The experiments are conducted to compare the efficiency from battery output to inverter output. The efficiency in the conventional method and the proposed method is measured under the condition that the torque command value was fixed at 20 Nm and 60 Nm. The secondary

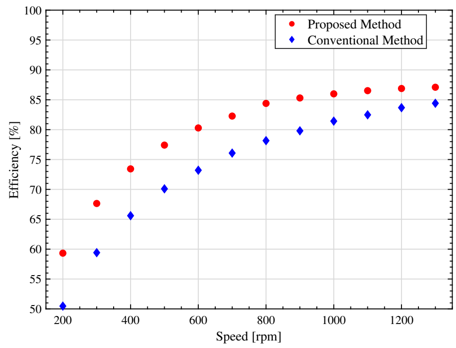

Fig. 13. Battery to inverter output efficiency in experiment. (torque is 20 Nm)

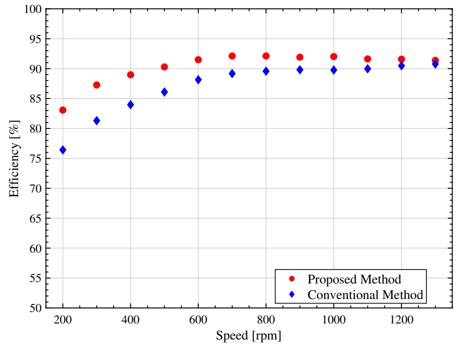

Fig. 14. Battery to inverter output efficiency in experiment. (torque is 60 Nm)

side DC-link voltage command is shown in Fig. 9. Efficiency was measured at the motor rotation speed from 200 rpm to 1300 rpm by every 100 rpm. The experimental results shown in Fig. 13 and Fig. 14 show the effectiveness of the proposed method. Since the switching loss of the AC/DC converter is not taken into consideration, the efficiency of the experiment result is worse than the simulation result. Especially in the low output range, the efficiency of proposed method is more efficient than conventional method because the ratio of the switching loss to the output power is large. In high torque and high speed range, the efficiency of the proposed method and that of the conventional method are almost the same. In this range, voltage command is restricted by WPT system. Therefore, the effect of the proposed method is weak.

7. Conclusion

In this research, maximum efficiency operation method by adjusting optimal secondary side DC-link voltage without extra back-boost converter is proposed. The experimental result shows the effectiveness of the proposed method. As a future work, there is a study of a method of improving WPT efficiency. WPT efficiency can be controlled by the voltage ratio between the primary side and the secondary side. V_{11}, the fundamental harmonics of v_{11}, can be also controlled by changing duty ratio of the 3-level wave. If V_{11} and V_{21} are adjustable respectively, WPT efficiency can be maximized by adjusting the voltage ratio to the optimum value.

8. Acknowledgements

The contributions of Toyo Denki Seizo K.K. and NSK Ltd. are gratefully acknowledged. This work was partly supported by JSPS KAKENHI Grant Number 18H03768 and JST-Mirai Program Grant Number JPMJMI17EM, Japan.

References

(1) Y. Hori, "Research on Future Vehicle driven by Electricity and Control," *IEEE Transactions on Industrial Electronics*, vol. 51, no. 5, pp. 954–962, 2004.
(2) N. Shimoya and H. Fujimoto, "Fundamental Study of Driving Force Distribution Method for Minimization ofMaximum Slip Ratio for Electric Vehicles with In-wheel Motors," *EVTeC & APE Japan*, 2016.
(3) T. Enmei, H. Fujimoto, Y. Hori, D. Gunji, and K. Omata, "Slip ratio control using load-side high-resolution encoder for in-wheel-motor with reduction gear," *International Conference on Mechatronics, ICM 2017*, 2017.
(4) S. Harada and H. Fujimoto, "Range extension control system for electric vehicles based on front and rear driving force distribution considering load transfer," *(IECON) 2013-39th Annual Conference of the IEEE*, vol. 39, pp. 6626 – 6631, 2013. [Online]. Available: http://ieeexplore.ieee.org/xpls/abs{_}all.jsp?arnumber=6119938
(5) Y. Ikezawa, H. Fujimoto, D. Kawano, Y. Goto, Y. Takeda, and S. Koji, "Range Extension Autonomous Driving for Electric Vehicle Based on Optimal Vehicle Velocity Profile in Consideration of Cornering," *IEEJ Transactions on Industry Applications*, vol. 137, no. 1, pp. 1–9, 2016.
(6) M. Sato, G. Yamamoto, T. Imura, and H. Fujimoto, "Experimental verification of wireless in-wheel motor using magnetic resonance coupling," *9th International Conference on Power Electronics - ECCE Asia: "Green World with Power Electronics", ICPE 2015-ECCE Asia*, pp. 1667–1672, 2015.
(7) M. Kato, T. Imura, and Y. Hori, "New characteristics analysis considering transmission distance and load variation in wireless power transfer via magnetic resonant coupling," *International Telecommunications Energy Conference*, 2012.
(8) D. Gunji and T. Imura, "Fundamental Research on Structure of Power Conversion Circuit and Control Method for Wireless In-Wheel Motor using Magnetic Resonance Coupling," *IECON 2014 - 40th Annual Conference of the IEEE Industrial Electronics Society*, vol. 2, 2014.
(9) M. Takeda, N. Motoi, and A. Kawamura, "Output Voltage Optimization of Interactive Boost and Back Chopper for Electrical Vehicles and its Evaluation," in *IEE-Japan Industry Applications Society Conference*, 2012, pp. 419–422.
(10) S. Morimoto, Y. Tong, and T. Hirasa, "Loss Minimization Control of Permanent Magnet Synchronous Motor Drives," *IEEE Transactions on Industrial Electronics*, vol. 41, no. 5, pp. 511–517, 1994.